doi:10.1017/S1431927617006419
Microsc. Microanal. 23 (Suppl 1), 2017


# Comparison of 3-D Cellular Imaging Techniques using Scanned Electron Probes

R.D. Leapman[1], E.L. McBride[1], A. Rao[1], G. Zhang[1], Q. He[1], M.D. Guay[1], I.D. Pokrovskaya[2], B. Storrie[2], M.A. Aronova[1]

[1.] National Institute of Biomedical Imaging and Bioengineering, NIH, Bethesda, MD
[2.] Department of Physiology and Biophysics, University of Arkansas for Medical Sciences, Little Rock, AR, USA

The use of scanned focused electron probes, rather than wide-beam illumination in the TEM, enables determination of 3-D cellular and tissue ultrastructure by taking advantage quantitatively of the physical interactions between incoming electrons and the specimen. Here, we compare the relative advantages of two techniques developed in the past decade, which are finding increasing applications: serial block face SEM [1], and STEM tomography [2].

In SBF-SEM, an ultramicrotome is built into the specimen stage of an SEM, and a low-energy (~1 keV) electron probe produces a backscattered electron signal from a thin layer below the surface of a heavy-atom stained, resin-embedded block. Due to the low average atomic number of the plastic block, scattering is in the forward direction, providing a lateral (*x*,*y*) resolution of around 5 nm, whereas the *z*-resolution is typically limited to minimum slice thickness of ~25 nm, although it is possible to improve the *z*-resolution by acquiring images at multiple beam energies [3, 4]. SBF-SEM can be used to determine ultrastructure of large (~$10^4$ – $10^6$ μm$^3$) volumes of biological specimens. In axial bright-field (BF) STEM tomography, a high-energy (~300 keV) probe of electrons is focused with a small convergence semi-angle of ~1 mrad into a ~2-nm diameter, providing a depth-of-field of ~2 μm in a thick section of a stained, embedded specimen. Unlike conventional TEM, there are no post-specimen lenses in STEM, so increased energy spread due to multiple inelastic scattering in thick specimens does not affect image quality due to chromatic aberration [2].

Previously, we have applied both SBF-SEM and STEM-tomography to determine cellular ultrastructure. Here, we compare performance of the two techniques in the analysis of human blood platelets, which are small, anucleate blood cells that maintain hemostasis and aggregate to seal leaks at sites of vascular injury. Platelets are critically important in the pathology of atherosclerosis and other diseases, and detailed visualization of cellular ultrastructure can help provide a higher understanding of platelet physiology [5, 6].

From our results (Figures 1 and 2) we can make some broader conclusions about the relative advantages of the two techniques [7]. The quality of 3-D data from human platelets, obtained with SBF-SEM is similar to that obtained with STEM tomography. Nevertheless, the higher spatial resolution of STEM tomography is able to reveal, on platelet activation, the formation of tubular extensions connecting decondensing alpha-granules to the plasma membrane and providing the only route for release. In resting cells, we found the canalicular system to be more closed than previously thought; and on activation, plasma membrane openings increased 2- to 3-fold [5].

On the other hand, SBF-SEM has important advantages despite its slightly lower spatial resolution. SBF-SEM provides 3-D data from much larger volumes ($10^3$–$10^6$ μm$^3$) than achievable with STEM tomography ($10^1$–$10^2$ μm$^3$). Data acquisition in the SBF-SEM can be performed automatically over

longer times than for STEM tomography. Processing time for manual segmentation scales with 3-D volume. However, in future, automated segmentation techniques are likely to reduce the processing time even for very large data sets. This provides a further advantage to SBF-SEM since segmentation is often the limiting factor in determining the amount of data that can be analyzed [8].

References:
[1] W. Denk and H. Horstmann, PloS Biol. **2** (2004) p. 1900.
[2] M.F. Hohmann-Marriott *et al*, Nature Methods **6** (2009) p. 729.
[3] F. Boughorbel *et al*, Microsc. Microanal. **19** (Suppl **2**) (2013) p. 380.
[4] Q. He *et al*, Biophys. J. **112** (**3**, Suppl **1**) (2017) p. 574a.
[5] I.D. Pokrovskaya *et al*, J. Throm. Haem. **14** (2016) p. 572.
[6] S. Yadav, *et al*, Platelets (2017) (in press) http://dx.doi.org/10.1080/09537104.2016.1235685
[7] E.L. McBride *et al*, Biophys. J. **112** (**3**, Suppl **1**) (2017) p. 574a.
[8] Research supported by the intramural program of NIBIB, NIH. Work in the Storrie laboratory was supported in part by NIH Grant R01 HL119393.

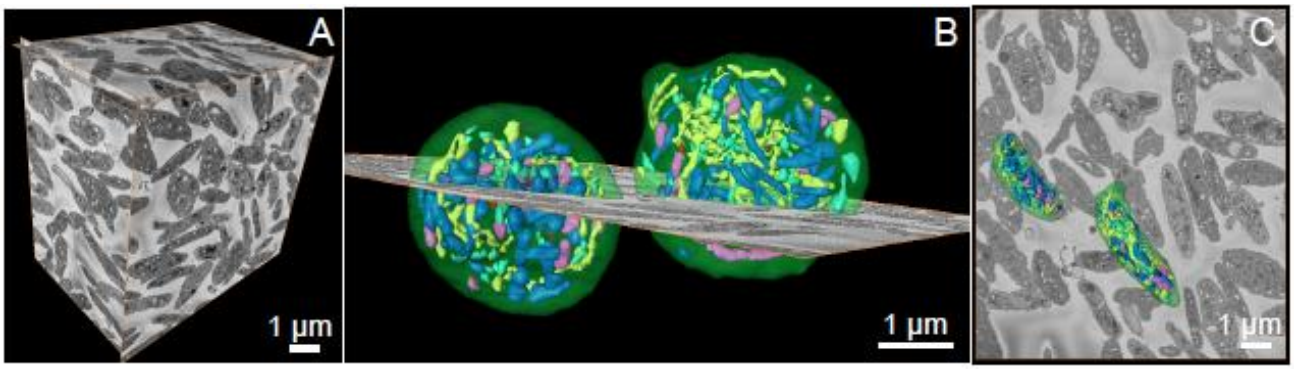


**Figure 1.** Visualization of non-activated human blood platelets obtained by SBF-SEM. 3-D volumes were obtained using a Zeiss Sigma VP SEM equipped with a Gatan 3View SBF system. Images were acquired with a beam energy of 1.1 keV with 5-nm pixels in the (x,y) plane and with cutting thickness of 30 nm in the z-direction. (A) Representation of 3-D data set containing >100 platelets; (B, C) different views of surface-rendered organelles in two complete platelets; open canalicular system (yellow), closed canalicular system (cyan), mitochondria (purple), alpha-granules (blue), dense core granules (red), plasma membrane (green).

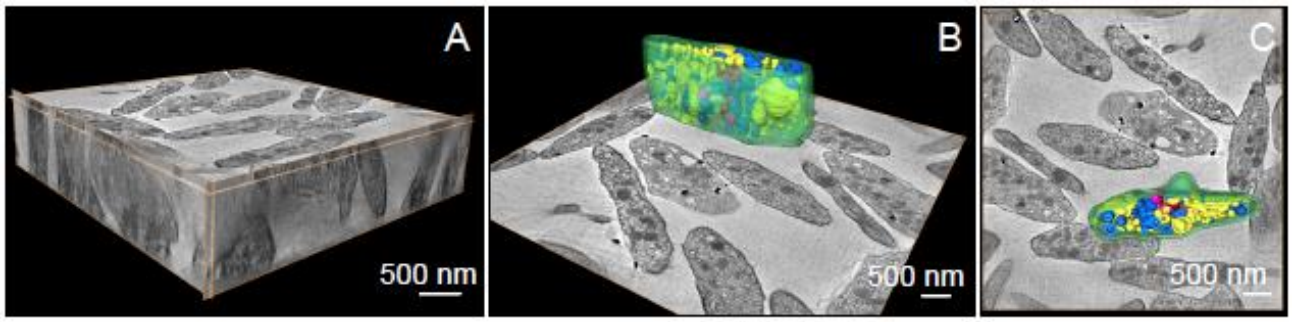


**Figure 2.** Comparison of 3-D structure obtained by STEM tomography. Images were acquired with an FEI Tecnai TF30 TEM, equipped with a Gatan BF/DF STEM detector by recording dual-axis bright-field STEM tomograms, with pixel size of 3 nm and tilt angles of ±68° with tilt increment of 2°. (A) Representation of 3-D data set containing ~10 platelets; (B, C) different views of surface-rendered organelles in one platelet, ~2/3 of which is contained in the 1.5-µm thick section. Color scheme for organelles is same as for Figure 1.

https://doi.org/10.1017/S1431927617006419 Published online by Cambridge University Press